Synthesis and low-order optical nonlinearities of colloidal HgSe quantum dots in the visible and near infrared ranges

Rashid A. Ganeev,[1,2,3,4,6] **Ivan A. Shuklov,**[2,*] **Andrey I. Zvyagin,**[1] **Dmitry V. Dyomkin,**[2] **Michail S. Smirnov,**[1] **Oleg V. Ovchinnikov,**[1] **Anna A. Lizunova,**[2] **Alexander M. Perepukhov,**[2] **Victor S. Popov,**[2] **and Vladimir F. Razumov**[2,5]

[1]*Department of Physics, Voronezh State University, Voronezh 394006, Russia*
[2]*Moscow Institute of Physics and Technology (National Research University), Dolgoprudny 141701, Russia*
[3]*Institute of Astronomy, University of Latvia, Riga, LV – 1586, Latvia*
[4]*American University of Sharjah, Sharjah, PO Box 26666, United Arab Emirates*
[5]*Institute of Problems of Chemical Physics, Russian Academy of Sciences, Chernogolovka 142432, Russia*
[6]*rashid_ganeev@mail.ru*
[*]*ivan.shuklov@gmx.de*

Abstract: We synthesize colloidal HgSe quantum dots and characterize their nonlinear refraction and nonlinear absorption using a Nd:YAG laser and its second harmonic. The 7.5 nm quantum dots were synthesized using the hot-injection method. The nonlinear absorption ($\beta = 9\times10^{-7}$ cm W^{-1}) and negative nonlinear refraction ($\gamma = -5\times10^{-12}$ cm^2 W^{-1}) coefficients of colloidal quantum dots were determined using the 10 ns, 532 nm laser radiation. The joint influence of above processes was realized at a higher intensity of probe pulses. In the case of 10 ns, 1064 nm radiation, only negative nonlinear refraction dominated during z-scans of these quantum dots. The studies of optical limiting using two laser sources demonstrated the effectiveness of this process at 532 nm. The role of nonlinear scattering is analyzed. We discuss the mechanisms responsible for the nonlinear refraction processes in colloidal HgSe quantum dots.

1. Introduction

The growing interest to quantum dot (QD) containing materials is attributed, particularly, due to their large low-order optical nonlinearities [1], which can be useful in photonics [2–4] and optoelectronic devices in different time scales [5,6]. QDs have properties intermediate between bulk semiconductors and discrete atoms or molecules. Their characteristics change as a function of both size and shape. For these reasons, novel synthesized semiconductor QDs require to be examined under different conditions using laser pulses of variable energies, wavelengths and durations to understand the nonlinear optical mechanisms and distinguish their attractive properties for practical applications [7,8].

Semiconductor nanoparticles (NPs) demonstrate various nonlinear optical phenomena [9–14]. In particular, colloidal semiconductor nanocrystals provide strong size-related optical and optoelectronic properties. QDs may show variable nonlinear optical properties at different pulse durations and wavelengths. When QDs are pumped by nanosecond laser at 532 nm wavelength, the most probable mechanism of nonlinear absorbance was assumed to be related with the reverse saturable absorption (RSA) [15]. However, when nanoparticles are excited by pico- and femtosecond laser pulses at wavelengths of 800 and 1064 nm, they can exhibit self-focusing effects, as well as negative and positive nonlinear absorption [16,17].

In recent years, there has been an increasing interest in the study of the nonlinear optical properties of semiconductor QDs with average sizes of less than 4 nm [18,19]. The main

advantages of such nonlinear optical media are high optical uniformity of the colloidal solution, as well as size-dependent spectral and luminescent properties. The dimensional dependence of the transition energy in absorption and luminescence opens up possibilities for achieving resonances, the use of which can reduce the threshold for optical nonlinearities [20]. The potential application of this effect is an efficient generation of high-order harmonics in the laser-induced plasmas containing such small-sized species [19,21].

The use of QDs with a certain set of localized states causes a strong influence on the formation of accumulative nonlinearities that occur when exposed to nanosecond pulses [22–24]. Among them are the resonant two-photon excitation and RSA, as well as the nonlinear refraction due to the zone filling effect caused by changes in the population of the dimensional quantization levels and local states in the QD. Such quantum dots include nanocrystals of non-stoichiometric compounds (PbS, Ag_2S, PbSe, etc.) that have a developed system of structural defects involved in the formation of nonlinear refraction.

Meanwhile, to the best of our knowledge, there are no studies devoted to the analysis of the low-order nonlinear optical properties of the mercury selenide (HgSe) colloidal QDs. Knowing the nonlinear optical refraction and absorption allows predicting the behavior of the response of these QDs in the case of relatively strong optical fields. This knowledge can be useful during optimization of the potential applications of HgSe QDs, particularly, as the efficient sources of coherent extreme ultraviolet radiation.

HgSe colloidal quantum dots allow tailoring their various physical properties by varying the size of semiconductor core with some additional tuning by modification of the ligand shell. Some of following size-related effects are described in [25]. Mercury selenide QDs have a band gap between 420 meV and –274 meV in accordance with different literature sources. Several research groups explored HgSe CQDs for the mid-IR photodetection. Such colloidal quantum dot will pave the way for the development of spin-based applications [26]. HgSe CQDs exhibit the emission at the telecommunication wavelength between 1.3 and 1.55 μm [27]. Mercury selenide is also suggested to be used as topological insulator, with potential for application in spintronics [28].

HgSe quantum dots with narrowband absorption into the mid infrared region were successfully synthesized and analyzed [29–31]. The doped HgSe colloidal quantum dots (CQDs) possess unique intraband transition, which occurs between the first two conduction band states $1S_e$ and $1P_e$ in the doped HgSe quantum dots. By tuning the size of the HgSe quantum dots, the peak absorption wavelength can be controlled. The application of the intraband transition for photoconductors was first demonstrated in the 3–5 μm ranges of mid infrared [29].

The short description of the synthesis of HgSe CQDs is presented in [32]. Here we present the detailed analysis of the preparation of these species to clarify the important peculiarities influencing the morphological properties of synthesized QDs. The reason of rather detailed description of the synthesis of our samples is related with the intension to show how the technology of HgSe QDs synthesis influences the nonlinear optical properties of these small-sized species.

Most of physical properties of such colloidal nanomaterials are the direct consequence of chemical composition like material of semiconductor core, Hg:Se ratio, composition of ligand shell, etc. The majority of these properties depend on the chemical preparation route and work-up procedure. The morphology of obtained nanocrystalls depends on the synthetic route as well. Notice that, to the best of our knowledge, the used procedure to prepare HgSe CQDs was yet reported. Our studies show that the nonlinear optical properties of HgSe CQDs can be modified depending on the rout of QDs synthesis. Therefore here we provide the chemical route to the studied HgSe CQDs. The detailed analysis of QDs formation at different conditions allows for determination of the relations between the morphological and nonlinear optical properties of different QDs.

Earlier, the study of optical limiting (OL) with metallic nanoparticles has attracted a tremendous amount of attention of due to its increased demand for protection against laser threats to sensors and human eyes. One major approach is the utilization of nanoparticles as optical limiters. NPs and, particularly, QDs have attracted much attention due to their high surface-to-volume ratio and quantum confinement. These nanocomposites have special nonlinear optical behavior as compared to the bulk materials. For instance, optical nonlinearities and OL effects of the nanocomposites of the metals can be significantly enhanced by increasing the number density and low dimensionality of the metal particles [33–35]. Additionally, NPs may display a drastic optical extinction due to their nonlinear scattering.

In this paper, we describe the synthesis of 4.5-, 7.5-, and 11-nm HgSe QDs using the hot-injection method and analyze strong nonlinear refraction and nonlinear absorption of these colloidal QDs using 532 nm, 10 ns laser pulses, while comparing with the nonlinear refraction at 1064 nm. The joint influence of above processes was realized at higher intensity of probe 532 nm pulses. We present the results of nonlinear scattering and optical limiting studies, which demonstrate the efficient limitation of the 532 nm radiation. We discuss the mechanism responsible for the nonlinear optical processes in these samples.

2. Synthesis and characterization of colloidal quantum dots

HgSe is frequently mentioned as semimetal with close to zero bandgap and therefore mercury selenide colloidal quantum dots (CQDs) could be the attractive material for the detection in near- and mid-IR spectral ranges [36–39]. Self-doped HgSe CQDs with intraband gap could form by many synthetic approaches. Such nanocrystals display strong mid-IR absorption between the lowest electron state $1S_e$ and the next level $1P_e$. Exact position of intraband absorption peak depends on the size of nanocrystalls and the ratio of reagents. Such materials possess photosensitivity in mid-IR and have shown promising photoelectric properties [40].

Synthesis of HgSe CQDs is frequently performed using the hot-injection method by an addition of selenium precursor to the mercury precursor prepared from mercury acetate, oleic acid and oleylamine. There are two preparation procedures for such mercury precursor possible: simultaneous mixing of all mentioned chemicals [41] and subsequent addition of oleic acid to mercury acetate followed by oleylamine [42]. One can expect the formation of mercury oleate solution in oleylamine in both cases. Notice that these two precursors, being at the first glance interchangeable, provide quite different results in the synthesis of HgSe CQDs. Surprisingly, these popular mercury precursors in Hg nanocrystals chemistry remain the uninvestigated ‚black boxes" in the literature up to now. This finding inspired us studying them more in details as part of our ongoing studies on the synthesis of chalcogenide CQDs [43–46].

2.1. Synthesis procedures

Following solvents and chemicals were used without additional purification: mercury acetate (99%, Acros), selenium (99.99%, Aldrich), trioctylphosphine (90%, Acros), oleic acid (90%, Aldrich), oleylamine (80-90%, Acros), hexane (99% HPLC grade, Macron Fine Chemicals), tetrachloroethene (TCE, 99%, Acros) и methanol (99%, HPLC grade, Khimmed). Oley-lamine(80–90%, Acros) was dried at 110 °C at reduced pressure (5 mbar) for 2 h. All reactions were carried out under argon atmosphere using Schlenk line techniques.

TOP-Se was prepared by adding selenium powder (0.39 g, 5 mmol) to 5 ml of trioctylphosphine (TOP) under argon (1 M solution) in a Schlenk tube. The mixture was stirred and heated to 70 °C for approximately 1 hour to fully dissolve the selenium powder, before being cooled to room temperature.

For synthesis based on mercury acetate, two approaches to the preparation of a mercury precursor were compared: with sequential mixing of mercury acetate with oleic acid and then with oleylamine (B) and simultaneous mixing of all these reagents (A).

A (subsequent loading). Hg(OAc)$_2$ (0.2 g, 0.6 mmol) and oleic acid (2 ml) were placed in 25 ml three necked-flask and stirred 30 min at 100 °C under argon. Oleylamine (6 ml) was added and r.m. was stirred another 30 minutes at 100 °C. 1M solution of TOP-Se in TOP (0.3 ml) was added to the reaction mixture at the desired synthesis temperature. Reaction mixture was quenched by an addition of 1 ml of 1-dodecanethiol followed immediately by cooling with ice bath. Colloidal quantum dots were purified by redispersing in TCE, followed by precipitation with methanol and centrifuging. QDs HgSe residue was dispersed in TCE for further characterization with Fourier transform infrared spectroscopy (FTIR) and transmission electron microscopy (TEM).

B (simultaneous addition). Hg(OAc)$_2$ (0.2 g, 0.6 mmol), oleic acid (2 ml) and oleylamine (6 ml) were placed in 25 ml three necked-flask and stirred 60 min at 100 °C under argon. 1M solution of TOP-Se in TOP (0.3 ml) was added to the reaction mixture at the desired synthesis temperature. Reaction mixture was quenched by an addition of 1 ml of 1-dodecanethiol followed immediately by cooling with ice bath. Colloidal quantum dots were purified by redispersing in TCE, followed by precipitation with methanol and centrifuging. QDs HgSe residue was dispersed in TCE for further characterization with FTIR and TEM.

2.2. Characterization of samples

Absorption spectrum of CQDs in the range between 410 and 1200 nm is presented in Fig. 1(a). Both used wavelengths of probe pulses (532 and 1064 nm) are within this range.
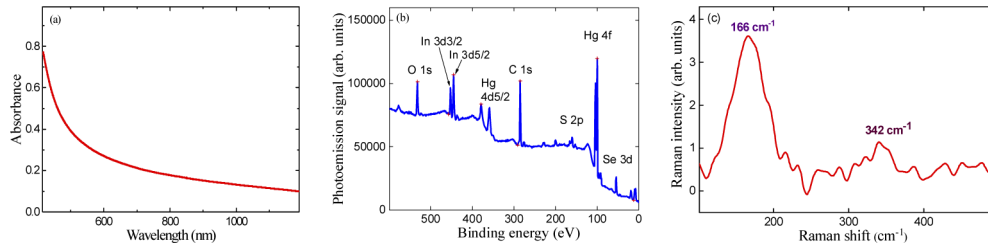

Fig. 1. (a) Absorbance of HgSe CQDs in the range of 420–1200 nm. (b) X-ray photoelectron spectroscopy. (c) Raman spectrum.

The chemical compositions were explored by X-ray photoelectron spectroscopy (XPS, PHOI-BOS 150 MCD, Specs) using Mg Ka radiation (1253.6 eV). Sample for XPS spectroscopy was prepared by drop-casting of HgSe CQDs solution in TCE on a 9×9 mm indium foil. The chemical composition of PbS QDs was confirmed by XPS, and the related spectrum is shown in Fig. 1(b). The peaks for Hg and Se along with C, S, In, and O from the product are observed in the XPS spectrum. The two strong peaks for the Hg region observed at 100.4 and 104.4 eV are assigned to the Hg(4f) binding energy. Peaks of S ($2p_{3/2}$ and $2p_{1/2}$) at ~165 eV confirm the presence of dodecanthiol-1 in ligand shell. The mercury and selenium ratio was found to be close to 1.2:1, which suggests that the obtained HgSe QDs were rich in Hg ions on the surface.

Sample for Raman spectroscopy was prepared by drop-casting of HgSe CQDs solution on 8×8 mm glass substrate. Raman spectrum was acquired from a nanoparticle film deposited on a glass substrate using a commercial DXR Raman microscope (ThermoFisher Scientific), a Si detector, and a 532 nm laser excitation. Figure 1(c) shows the low energy Raman spectrum for the HgSe CQDs film. The spectrum represents two broad phonon signals of HgSe (at 166 and 345 cm^{-1}).

2.3. Investigation of the HgSe CQDs synthesis approaches using various mercury precursors and characterization of samples

We compared the precursors obtained by subsequent (method A) and simultaneous (method B) addition. Firstly, we studied the dependence of HgSe CQDs optical properties for both mercury precursors on the reaction temperature (Table 1). Synthesis at 100 °C provides the best results in terms of intraband transition peak broadening and colloidal stability of obtained samples. Both methods at this temperature provide colloidal solutions of HgSe CQDs with good long-term colloidal stability and intraband absorption peak at the wavelength ~4.7 µm (Fig. 2). Note that the subsequent addition resulted in samples formation with narrower intraband absorption peak (FWHM ≈ 1120 nm). Increasing of reaction temperature up to 120 °C decreases the long-term colloidal stability of obtained samples. Intraband absorption peak undergoes further red shift up to 10 µm and broadens significantly (FWHM ~ 5700 nm). Synthesis of HgSe CQDs at 80 °C allows obtaining the long-term stable colloidal solutions with very broad intraband absorption peak (FWHM ≥ 5000 nm).
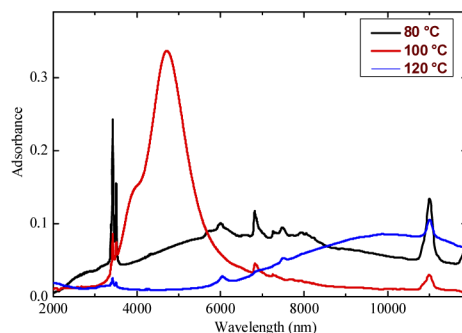

Fig. 2. Absorption spectra of HgSe QDs synthesized by method A at various temperatures.

Table 1. Synthesis of HgSe CQDs by variation of the temperature of mercury precursor

Hg-precursor	Temperature, °C		
	80	100	120
A	λ ~ 6.3 µm FWHM ≥ 5000 nm	λ ~ 4.7 µm FWHM ≈ 1120 nm	λ ~ 10 µm[a] FWHM ~ 5700 nm
B	-	λ ~5.6 µm[a] FWHM ≈ 2640 nm	λ ~ 7600 µm[a] FWHM ≈ 2520 nm

[a]poor colloidal stability

The mean particle sizes and particle size distributions of synthesized HgSe quantum dots were determined by TEM measurements (Fig. 3). The samples prepared at 80 °C showed mean size of QDs about 5 nm with poorly formed spherical particles. The best particle size distribution and well-formed spherical nanocrystalls with mean diameter of 7.5 nm was obtained at 100 °C. Further increase of temperature up to 120 °C led to formation of larger nanocrystals with mean size of 11 nm and worse particle size distribution.

IR spectroscopy and nuclear magnetic resonance spectroscopy (^{1}H NMR) confirm the presence of dodecanethiol in the ligand shell (Figs. 4(a) and 4(b)). C-H valence vibrations of CH_2 and CH_3 groups could be observed in FTIR spectra at 2800-2900 cm^{-1} as well as CH_2 bending at 1460 cm^{-1}. ^{1}H NMR spectra reveals signals from aliphatic protons of dodecanethiol (DDT) alkyl chain at 0.5–2 ppm. CH_2-S adjacent to the semiconductor core is not visible in ^{1}H NMR. Olefinic protons belonging to the oleic acid or oleylamine could be detected at 5.5 ppm in tiny amounts.
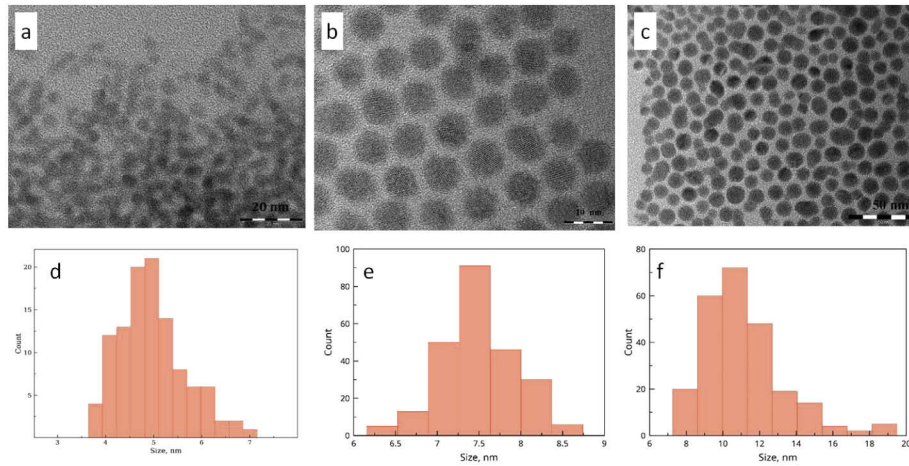
Fig. 3. TEM images ((a), (b) and (c)) and histograms ((d), (e) and (f)) of HgSe CQDs obtained during synthesis at 80 °C ((a) and (d)), 100 °C ((b) and (e)), and 120 °C ((c) and (f)). Line markers in TEM images correspond to 20 nm (a), 10 nm (b) and 50 nm (c).

Diffusion ordered spectroscopy has shown that these protons belong to a free substances or highly labile very weakly bounded ligands.
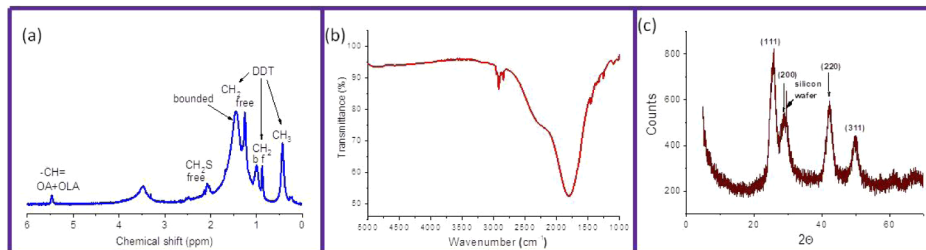

Fig. 4. (a) ^{1}H NMR and (b) FTIR spectra of HgSe CQDs synthesized at 100 °C by method A. (c) XRD of HgSe CQDs.

X-ray diffraction (XRD) on the particles prepared at 80 °C confirmed the cubic zinc blende structure of the HgSe colloidal quantum dots (Fig. 4(c)) similar to those shown in recent reports on the synthesis of HgSe nanostructures [47]. The broad XRD lines serve as an evidence of nanocrystalline nature of the material. Accoding to Debye–Scherrer equation the average crystalline size at 80 °C is estimated to be a 4.5 nm.

The energy of intraband gap in HgSe colloidal quantum dots depends on their sizes, size distribution and the ratio of Hg to Se on the quantum dot core surface [25]. We studied the dependence of intraband absorption peak position and broadness on the ratio of applied mercury and selenium precursors. Higher amount of mercury precursor in reaction mixture results in the blue shift of intraband absorption peak from 4.7 μm for Hg:Se ratio 1:1 to 3.7 μm at ratio 2:1 (Table 2).

Position of extreme broad absorption peak in the CQDs synthesized at 80 °C remained almost unchanged (6.3 μm vs 6.5 μm) for both Hg:Se ratios. Excess of selenium had negative impact at all tested temperatures. At 80 °C obtained at ratio 1:2 Hg:Se colloidal nanocrystalls do not have any intraband and interband absorption peaks in the range between 0.2 μm to 12 μm. We failed to obtain colloidal solutions with excess of selenium at higher temperatures. We also found that a

Table 2. Dependence of the intraband absorption peak maximum on the Hg:Se ratio.

Hg:Se ratio	Temperature		
	80 °C	100 °C	120 °C
2:1	~ 6.5 μm	3.7 μm	-
1:1	~ 6.3 μm	4.7 μm	10 μm
1:2	_[a]	_[b]	-

[a]no intraband absorption peak
[b]colloidal solution was not formed.

prolonged heating at temperatures above 100 °C during mercury precursor preparation leads to the formation of large amounts of metallic mercury as a side product.

3. Nonlinear optical studies of QDs

3.1. Method

In the following studies, we used the samples prepared at 100 °C, with 7.5 nm mean sizes of QDs. Studies of the nonlinear optical properties of HgSe QDs were performed by z-scan technique. The main idea of this technique is to measure the change in incident Gaussian laser beam intensity during transmission through the sample as a function of its position (z-position) with regard to the focal plane of the beam. Transmitted beam is collected by means of two detector arrangements: closed-aperture in order to recognize the sign and measure the nonlinear refractive index (γ) and open-aperture scheme in order to measure the nonlinear absorption coefficient (β). The working principle of z-scan technique is based on the motion of the sample along the z-axis from $-z$ to $+z$ through the focus of a tightly focused Gaussian laser beam. The motion of the sample across the focused beam exposes it to a varying irradiance (intensity) level reaching its maximum value at the focus point.

In most of experiments we used the second harmonic of the Nd:YAG laser (pulse duration 10 ns, pulse repetition rate 1 Hz) with $\lambda = 532$ nm obtained using a KDP crystal. We also used the fundamental radiation of this laser (1064 nm) for the studies of the optical nonlinearities of QDs in the near IR region. Laser radiation was focused with a 300 mm focal length spherical lens (inset in Fig. 5(a)). The beam waist diameters were 80 μm and 60 μm (at half width of $1/e^2$ maximum of the spatial distribution at the focal plane) in the case of fundamental and second harmonic beams respectively. The 0.2-mm-thick fused silica cells containing CQDs were moved along the z-axis through the focal point using a translating stage controlled by a computer. The energy of the laser pulse was measured with a calibrated photodiode and registered with a digital voltmeter. The energy of the pulses used in the experiment excluded optical breakdown of the studied samples. The intensity of 532 nm radiation used in the experiments did not exceed 4×10^8 W cm^{-2}.

Special attention was paid to the closed aperture (CA) z-scans. To obtain them, the 1-mm aperture was fixed at a distance of 150 cm from the focal plane, behind which the second photodiode was located. The ratio of the transmitted radiation registered by the second photodiode and the incident radiation registered by the first photodiode was taken as the normalized transmission. Away from the focal point, where nonlinear processes do not occur, the normalized transmission was 1. This made it possible to avoid the influence of instability of the laser radiation on the results obtained. Each point on the experimental dependencies corresponds to an average of 20 measurements. The scheme with CA allowed determining the sign and value of the nonlinear refractive index of the QD-containing medium. The open-aperture (OA) scheme
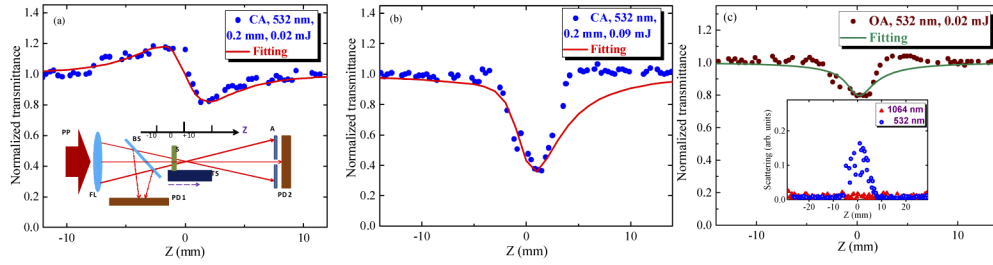
Fig. 5. (a) CA z-scan using 0.02 mJ pulses. Inset shows the z-scan scheme used in these studies. PP, probe pulse; FL, focusing lens; BS, beamsplitter; S, sample; TS, translating stage; A, aperture; PD1 and PD2, photodiodes. (b) CA z-scans using 0.09 mJ pulses. (c) OA z-scan using 0.02 mJ pulses. Aperture in that case was removed from the pass of probe pulse to collect the whole amount of propagated radiation. Inset: scattered signal as a function of sample position in the case of 532 nm (blue circles) and 1064 nm (red triangles). Solid curves in these figures correspond to the fittings using Eqs. (2) and (3).

allowed determination of the nonlinear absorption of the samples. The z-scan scheme was calibrated using the known values of the nonlinear optical parameters of 1-mm-thick quartz. The error bars of the definition of the absolute values of nonlinear optical parameters were estimated to be ±25% due to the uncertainty in the measurements of the intensities of laser pulses in the focal plane.

The optical limiting studies were carried out by varying the energy of the pulses propagating through the cells. The energy was changed using the calibrated filters. The sample was placed on the path of focused radiation at the position when energy density was sufficient for observation of optical limiting. We also carried out the nonlinear scattering studies of HgSe CQDs.

The optical damage thresholds of CQDs using 10 ns, 532 nm and 10 ns, 1064 nm probe pulses were determined to be 6×10^9 and 9×10^9 W cm^{-2}, respectively. These values of optical damage were more than one order of magnitude larger than the intensities used during our measurements of the optical nonlinearities of samples.

3.2. Measurements of optical nonlinearities using 532 and 1064 nm radiation

Figure 5(a) shows the CA z-scan of HgSe CQDs (C=2.4×10^{-5} M, which corresponded to the concentration of QDs equal to 1.4×10^{16} cm^{-3}) using 0.02 mJ, 532 nm, 10 ns probe pulses. This dependence of the normalized transmittance (T) of 0.2 mm thick cell filled with CQDs on its position along the z-axis demonstrates that the peak (T=1.18) and valley (T=0.8) of this curve were almost equal to each other with regard to T=1. One can assume that only the negative nonlinear refraction, when peak follows by valley, plays the decisive role at these experimental conditions. Our experiments were carried out at small pulse repetition rate (1 Hz), when the accumulative thermal processes leading to the formation of negative nonlinear refraction play insignificant role, thus demonstrating the prevailing role of Kerr-related process.

The z-scan scheme was calibrated using the known value of quartz (3.3×10^{-16} cm^2 W^{-1} [48]). The following simplified equation can be used for calculation of the nonlinear refractive index of the sample at the conditions when the role of nonlinear absorptive effects becomes insignificant [49]: $\Delta T_{pv} \approx 0.4(1-S)^{0.25} |\Delta\Phi|$. Here ΔT_{pv} is the normalized difference between peak-to-value transmission, S is the transmission of the aperture, $\Delta\Phi = k\gamma I_0 L_{eff}$, $k = 2\pi/\lambda$, λ is the radiation wavelength, I_0 is the laser radiation intensity in the focal plane, $L_{eff} = [1 - \exp(-\alpha L)]/\alpha$ is the effective length of the sample, α is the linear absorption coefficient, and L is the sample length. In the case shown in Fig. 4(a) ($\Delta T_{pv} \approx 0.4$, $I_0 = 8\times10^7$ W cm^{-2}, S = 0.1, $L_{eff} \approx 0.2$ mm, $\lambda = 532$ nm) the value of γ was determined to be -5×10^{-12} cm^2 W^{-1}. The figure of merit |γ/C|(C is the molar

concentration) of this colloidal suspension was calculated to be 2×10^{-7} cm^2 W^{-1} M^{-1}. The real part of nonlinear susceptibility of colloidal quantum dots (10^{-13} esu) was determined from the relation Re$\chi^{(3)} = |10^{-6}cn^2{}_0\gamma/480\pi^2|$, where n_0 is a linear refractive index of suspension ($n_0 \approx 1.6$).

The 4.5-fold increase of the pulse energy (0.09 mJ, Fig. 5(b)) drastically changed the z-scan and notably downplayed the role of nonlinear refraction compared with the nonlinear absorption. The peak was entirely removed, while demonstrating the asymmetric pattern with deep valley ($T\approx0.4$) with respect to the focal plane of the focusing lens.

The z-scans showing joint influence of nonlinear refractive and absorptive processes were analyzed by fitting the theoretical curve for the transmittance T with experimental dependencies [50]:

$$T(x) = 1 + \frac{4x}{(x^2 + 9)(x^2 + 1)}\Delta\Phi - \frac{2(x^2 + 3)}{(x^2 + 9)(x^2 + 1)}\Delta\Psi. \tag{1}$$

Here $x = z/z_0$, z_0 is the Rayleigh length of the focused radiation, $z_0 = 0.5k(w_0)^2$, w_0 is the beam radius at the $1/e^2$ level of the spatial intensity distribution in the focal plane, and $\Delta\Psi = \beta I_0 L_{\text{eff}}/2$ is the parameter determining phase shift near the focal point as a result of nonlinear absorption. The radius of the 532 nm beam waist was 30 μm. If there was no nonlinear absorption, or it too small, the third term in expression (1) was assumed to be close to zero when fitting z-scans (Fig. 5(a)). However, in the presence of nonlinear absorption, like in the case shown in Fig. 5(b), one has to modify Eq. (1) to make it suitable for fitting of the asymmetric curve. The presence of either two-photon absorption (TPA) or RSA enhanced the valley and suppresses the peak as presented in Fig. 5(b).

By making the substitution $\rho=\beta/2k\gamma$, one can get the relation between $\Delta\Phi$ and $\Delta\Psi$ ($\Delta\Psi=\rho\Delta\Phi$). In that case Eq. (1) can be re-written as follows:

$$T = 1 + \frac{2(-\rho x^2 + 2x - 3\rho)}{(x^2 + 9)(x^2 + 1)}\Delta\Phi_o. \tag{2}$$

The fittings using Eq. (2) shown in Figs. 5(a) and 5(b) allowed determining the nonlinear refractive index ($\gamma = -8\times10^{-12}$ cm^2 W^{-1}) and nonlinear absorption coefficient ($\beta = 6\times10^{-7}$ cm W^{-1}) of colloidal quantum dots in the case of 10 ns, 532 nm probe pulses. The difference in the measured values of γ retrieved from the symmetric and asymmetric z-scans (Figs. 5(a) and 5(b)) is attributed to the larger uncertainty in the accuracy of fitting procedure in the latter case.

Notice that the accuracy in determination of the nonlinear absorption coefficients using the OA z-scans is better compared with the CA z-scans, thus prompting us analyzing this process using the former configuration. The normalized transmittance in the case of nonlinear absorption for the OA z-scan is given by [51]

$$T(z) = (q)^{-1}ln(1 + q), \tag{3}$$

where $q=\beta I_0 L_{\text{eff}}/(1+z^2/z_0{}^2)$. The linear absorption in the case of 1064 and 532 nm wavelengths was measured to be 0.08 and 0.25 cm^{-1} for CQD, respectively. Correspondingly, in the case of these two wavelengths of the probe pulses propagating through the thin (0.2 mm) samples, the effective lengths of samples were almost similar to L. Thus the absorbance of studied samples does not affects the definition of β and γ when we assume that $L_{\text{eff}} \approx L$.

Figure 5(c) shows the OA z-scan of CQD using 0.02 mJ, 10 ns, 532 nm pulses and the fitting curve to those measurements. The nonlinear absorption coefficient ($\beta = 9\times10^{-7}$ cm W^{-1}) of colloidal quantum dots determined from this fitting was 1.5 times higher than the one determined from the CA measurements. The difference in these measurements was probably related with some inaccuracy in determination of the depth of valley during fitting procedure of CA z-scans of the joint influence of two nonlinear optical processes (Fig. 5(b)).

Similar OA measurements using 1064 nm pulses at the same pulse energy (0.02 mJ) did not show the valley in this curve thus demonstrating the absence of nonlinear absorption processes in CQD at this wavelength using weak laser pulses (Fig. 6(a)). The absorption spectrum of CQDs in the visible and near infrared ranges showed the small linear absorbance at 1064 nm (inset in Fig. 6(a)), which allow predicting the absence of the peculiarities of OA z-scan in the vicinity of z=0 at this energy of the probe pulses (Fig. 6(a)). The influence of nonlinear absorption can be observed only in the case of notably stronger pulses.
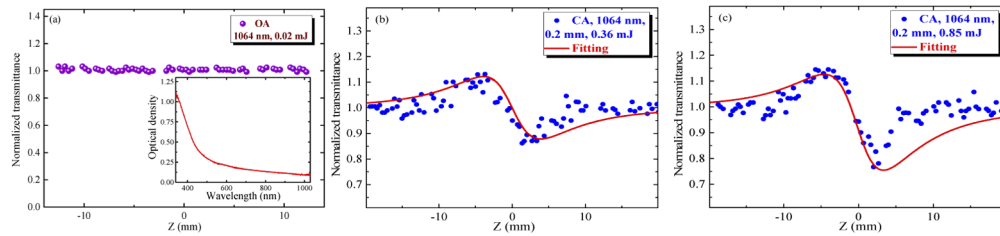

Fig. 6. (a) OA z-scan of CQDs using 0.02 mJ, 1064 nm pulses. Inset: linear absorbance of samples in the visible and near infrared ranges. ((b) CA z-scan of CQDs using 0.36 mJ, 1064 nm pulses. (c) OA z-scan of CQDs using 0.85 mJ, 1064 nm pulses. Solid curves in these figures correspond to the fittings using Eq. (2).

The nonlinear optical processes in this sample in the case of near infrared (1064 nm) radiation were observed only at considerably stronger probe pulses. CA z-scans of CQDs using 0.36 mJ, 1064 nm pulses also revealed the negative sign of nonlinear refraction (Fig. 6(b)), like in the case of 532 nm radiation. The symmetrical pattern of this curve was changed only in the case of more than twice higher energy of probe pulses (Fig. 6(c)), with valley larger than peak. The influence of nonlinear absorption in that case can be attributed to TPA. The fittings presented in Figs. 6(b) and 6(c) allowed determining the nonlinear optical parameters of HgSe CQDs at this wavelength of probe pulses (γ = -2×10^{-13} cm^2 W^{-1}, β = 4×10^{-9} cm W^{-1}). One can see that nonlinear absorption in that case can be revealed only at relatively high energies (and correspondingly intensities) of 1064 nm pulses (compare the results obtained from Figs. 5(a,b) and 6(c)).

3.3. Optical limiting studies

The investigation of optical limiting in various materials opens new opportunities for their application as laser switching systems for protection of eyes and sensitive registrars from intense laser radiation. Below we present our studies of OL in CQDs using 532 and 1064 nm probe radiation. The OL curve shown in Fig. 7(a) for HgSe QDs demonstrates a decay of transmittance with the increase of 532 nm probe pulse intensity starting from 0.8×10^6 W cm^{-2} up to 10^7 W cm^{-2}. The linear dependence between the input and output pulses was sustained up to the OL threshold (0.8×10^6 W cm^{-2}). The limiting of propagated 532 nm radiation is attributed to the influence of RSA and/or nonlinear scattering. At stronger intensities of probe pulses, some additional nonlinear optical processes can probably play important role. Another reason for the change in the OL profile is the process of saturable absorption at fluence higher than 0.1 J cm^{-2} (I_0 = 10^7 W cm^{-2}).

The TPA in metal NPs and semiconductor QDs is known to be accompanied by the formation of free carriers, which also contribute to the nonlinear character of light propagation in these media. The interaction of the propagating radiation with these newly formed charge carriers can result in self-defocusing, especially, in the case of longer probe pulses. In these experiments we have shown that excited state absorption in the visible range can be significant and needs to be considered in the case of even weakly absorbing clusters.
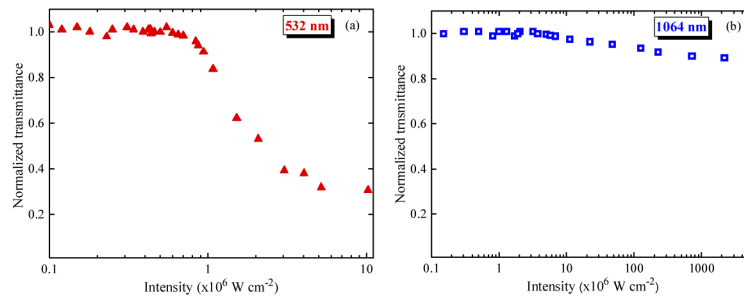
Fig. 7. Normalized transmittances at different intensities of probe pulses during OL studies using (a) 532 nm and (b) 1064 nm radiation.

Investigation of OL was also carried out at the 1064 nm wavelength (Fig. 7(b)). The sample showed very weak OL, though we analyzed this process using significantly stronger intensity (up to 4×10^9 W cm^{-2}). This peculiarity allowed us to assess how medium self-action properties influence OL in the near infrared range. Thus the propagation factors in these OL studies, i.e. ratios of transmittances at smallest and highest used intensities, were 2.5 and 1.1 in the case of 532 nm and 1064 nm pulses, respectively.

The optical, nonlinear optical and OL properties of small-sized species strongly depend on their size and shape as well as plasmonic resonances related with absorption peaks. Since the intraband absorption peak for mercury selenide (~5 μm) does not match with the wavelengths of probe pulses, the influence this resonance on the nonlinear refractive indices and nonlinear absorption coefficients at 532 and 1064 nm tends to be insignificant. During our studies, when the incident energy of 532 nm pulses was increased above the threshold at which the OL effect starts to dominate, the transmitted energy tended to approach a steady value.

There is the possibility of dynamic scattering of the laser beam by the CQDs, as well as the possibility of their photochemical transformation into structures of a different morphology [52]. To analyze the contribution to the z-scan from nonlinear dynamic scattering, a scheme was used in which a third photodiode was installed at an angle of 30^0 with regard to the optical axis of the probe pulses, close to the second photodiode (PD2, inset in Fig. 5(a)).

We observed some scattering in the case of 532 nm probe pulses, while no scattered signal was detected after the CQD-contained cell when we used the 1064 nm radiation. The inset in Fig. 5(c) shows the pattern of increased dynamic scattering in the focal plane of 532 nm radiation, probably due to the relatively large sizes of QDs (7.5 nm). At the same time, there is no reason to expect the significant influence of this process in the conditions used, since the RSA could adequately be considered as the cause of the observed patterns in the focal region in the case of relatively high energy flows of nanosecond 532 nm pulses. Thus the nonlinear scattering cannot be considered as the prevailing mechanism of the optical limiting at this wavelength. The inset also shows the almost insignificant nonlinear scattering using 1064 nm pump. Note that similar observation has been reported during nonlinear optical studies of the silver triangle NPs [53]. It was reported that the dynamic scattering in the case of strong laser radiation, which may contribute to the formation of a symmetric dip in the z-scan when samples with nanoparticles approach the focal plane, can modify the OA z-scans of small-sized species.

4. Discussion

During last time, different types of nonlinear optical materials emerged to broaden the range of potential 2D samples for different applications. Among them is a bismuthene based on the allotropes of Bi such as α-Bi and β-Bi, etc. Bismuth atoms are connected with the three atoms around them through covalent bonds, thus forming a low-buckled honeycomb structure [54].

Studies have shown that when the number of layers is reduced to below 22, bismuth will show the property of topological insulator; when the number of layers is less than 8, it will show the quantum spin Hall phase, and in the case of single layer Bi shows the property of semiconductor [55].

Another attractive 2D material is antimonene. Antimony has a buckled honeycomb structure and exhibits outstanding properties such as strong spin-orbit coupling, excellent thermal conductivity and high carrier mobility. These excellent properties of antimony have attracted scientists to further study their nonlinear optical properties. The dual wavelength mode-locking using antimonene-based saturable absorbers, which was a solid step forward in the application of the generation of terahertz waves using antimonene, was implemented in [56]. Antimonene, is a new type of 2D material beyond phosphorene, which is theoretically predicted to exhibit remarkable electronics and optical properties with enhanced stability. The nonlinear optical response of antimonene is investigated at the visible wavelength, which have shown that this material possesses a giant nonlinear refractive index of $\approx 10^{-5}$ cm^2 W^{-1} and a high stability in ambient conditions [57].

Among other developed 2D materials showing interesting nonlinear optical properties are tellurene [58] and graphdiyne [59]. Particularly, graphdiyne is a new carbon allotrope comprising sp- and sp^2-hybridized carbon atoms arranged in a 2D layered structure. 2D graphdiyne is demonstrated to exhibit a strong light–matter interaction with high stability to achieve a broadband Kerr nonlinear optical response, which is useful for nonreciprocal light propagation in passive photonic diodes. Graphdiyne has demonstrated a large nonlinear refractive index in the order of $\approx 10^{-5}$ cm^2 W^{-1}, comparing favorably to that of graphene.

All these species belong to mono-elemental analogs of black phosphorus [60]. It is difficult to compare the properties of those newly emerged media and our samples. To compare them at identical conditions one has to chose optimal spectral range, which is most suitable for demonstration of the outstanding nonlinear optical properties of each of comparing structures.

Our main results reported in this manuscript were retrieved using the 7.5-nm QDs, since these samples demonstrated the best stability, homogeneity, extended period of the maintenance of morphological, spectral, and stability characteristics compared with 4.5- and 11-nm species. To not overload the manuscript with numerous similar z-scans we included only those corresponded to the species demonstrated best morphological and stability characteristics (i.e. 7.5-nm QDs). However, the comparative nonlinear optical study of two groups of QDs differing in sizes was made as well, when we measured the nonlinear optical properties of 4.5- and 7.5-nm QDs synthesized during these studies. The highest values of nonlinear refractive indices and nonlinear absorption coefficients were observed in the case of the 7.5-nm species synthesized at 100 ºC.

The particular reason of the behavior when the nonlinear optical parameters of QDs increase with the increase of their size until some value is a subject for further investigation. Notice that similar effect has been demonstrated in [61]. They reported the approximately quadratic dependence of the hyperpolarizability of the QDs of different sizes. The growth of the nonlinear optical response with the increase of the sizes of QDs becomes a common feature of these species. The reason for this effect could be as follows. The incomplete passivation of the QD surface forms so-called surface trap states. Photoexcited carriers trapped at the QD surface form a static internal field leading to the saturation of the absorption. Our results qualitatively corroborate with above finding.

TPA can be concurrent to the RSA for CQDs in the case of the radiation wavelength used (1064 nm), since absorption at the surface plasmon resonance wing, though possible with the participation of single photon, seems less influential. Since intraband peak of HgSe CQDs was in the mid-infrared range, one can assume the influence of interband transitions on the TPA of 1064 nm pulses. Note the absence of the data on the spectral and energy properties of localized states and the possibility of their participation in transitions leading to the appearance

of nonlinear refraction. Thus, the above analysis indicates the absence of unambiguous criteria for the occurrence, mechanisms, and signs of nonlinear refraction for quantum dots, in particular for HgSe QDs.

The Kramers-Kronig model provides some clues in definition of the sign transformation of γ from self-focusing to self-defocusing and vice versa once one uses different wavelengths of probe pulses. The crucial parameter in this model is the band gap value of semiconductor. Below we address the modification of the sign of nonlinear refractive index using the Kramers-Kronig relations for the studied QDs.

An important characteristic of QDs is the band gap controllable by the size effect. This peculiarity of QDs can strongly change their nonlinear optical properties, in particular the sign of nonlinear refraction. The analysis of the nonlinear refraction of our CQDs shows that they demonstrate self-defocusing properties (Figs. 5 and 6) in the case of both 532 and 1064 nm probe pulses. The nonlinear Kramers–Kronig relations predict the self-defocusing in semiconductors for which the relation $\hbar\omega/E_g > 0.69$ takes place [62]. Here $\hbar$ is the Planck's constant, ω is the frequency of laser radiation, and E_g is the bandgap energy of semiconductor (<0.2 eV in the case of HgSe QDs [63]).

Meanwhile, once the sizes of semiconductor decrease below ~5 nm their band gap can be increased. It is not clear whether it is correct to consider HgSe QDs as semiconductors; however, some assumptions can be retrieved once one considers the similarity of some properties of different morphological structures containing similar elemental components. The corresponding $\hbar\omega/E_g$ values for our CQDs at the used wavelengths of probe pulses were calculated to be notably larger than 0.69. Thus, one can expect a negative sign of γ in these QD containing suspensions, which was confirmed in our experiments using 532 and 1064 nm probe pulses. The reason of relatively large value of nonlinear refractive index of HgSe CQDs at 532 nm (-5×10^{-12} cm^2 W^{-1}) can be related with the large value of $\hbar\omega/E_g$ (>30) compared with 0.69, at which the value of γ can be close to zero.

Our studies of HgSe CQDs demonstrated the domination of nonlinear absorption over nonlinear refraction. The Stegeman figure of merit $T_S = |2\beta\lambda/\gamma|$ [64] for the studied samples also shows the prevailing influence of nonlinear absorptive properties of used QD suspensions over their nonlinear refraction ($T_S \approx 19$ and 4 in the case of 532 nm and 1064 nm probe radiation, respectively). Note that the optical nonlinearities of the main liquid component of CQD suspension (tetrachloroethene) were significantly smaller ($>10^3$ times) compared with the nonlinearities of CQDs.

We analyzed the CA z-scans measured at two fluencies F (or intensities I) of the probe 532 nm pulses [F=0.7 J cm^{-2} (I=7$\times 10^7$ W cm^{-2}) and F=3.1 J cm^{-2} (I=3.1$\times 10^8$ W cm^{-2})], respectively (Figs. 5(a) and 54(b)). The 4.5-fold difference in the used intensities allowed us concluding about some increase of the negative nonlinear absorption index (from γ=-5$\times 10^{-12}$ to γ=-8$\times 10^{-12}$ cm^2 W^{-1}). Notice that, with the increase of the probe pulse intensity, the additional nonlinear optical effect (either TPA or RSA) starts playing the dominant role (Fig. 4(b)) at which the determination of lesser influencing process (i.e. nonlinear refraction) will have larger error bars. Meanwhile, the use of twice smaller energy of pulses (0.01 mJ), which corresponded to F=0.35 J cm^{-2} (I=3.5$\times 10^7$ W cm^{-2}), showed that the γ remained same as in the case of 0.02 mJ probe pulses. The same can be said about the measurements of the nonlinear absorption coefficient (Fig. 5(c)). Our analysis of the OA z-scan measured at the fluence F=0.7 J cm^{-2} (or intensity I=7$\times 10^7$ W cm^{-2}) of the probe 532 nm pulses allowed determining $\beta = 9 \times 10^{-7}$ cm W^{-1}. The 2-fold decrease of the probe pulse intensity did not lead to the variation of the nonlinear absorption coefficient.

The nonlinear optical parameters of studied CQDs at two wavelengths (532 nm and 1064 nm) are summarized in Table 3.

To measure the higher-order nonlinearities one has to determine the conditions suitable for the three- or four-photon absorption of the studied CQDs. At the used intensities of probe pulses neither of such processes was observed. Their influence will be manifested with the narrowing of

Table 3. Summary of the nonlinear optical measurements of HgSe CQDs. γ is the nonlinear refraction index, β is the nonlinear absorption coefficient, $\text{Re}\chi^{(3)}$ is the real part of third-order suspectibility, $\hbar$ is the Planck's constant, ω is the frequency of laser radiation, E_g is the bandgap energy of QDs, T_S is the Stegeman figure of merit, λ is the wavelength of laser radiation, C is the molar concentration, OL factor is the ratio of input laser energy and propagated laser energy at the maximal limiting observed in these studies.

	Size of QDs	γ	β	$\lvert\text{Re}\chi^{(3)}\rvert$	$\hbar\omega/E_g$	$T_S = \lvert 2\beta\lambda/\gamma\rvert$	$\lvert\gamma/C\rvert$	OL factor
532 nm	7.5 nm	-5×10^{-12} cm^2 W^{-1}	9×10^{-7} cm W^{-1}	1×10^{-13} esu	>30	19	2×10^{-7} cm^2 W^{-1} M^{-1}	4
1064 nm	7.5 nm	-2×10^{-13} cm^2 W^{-1}	4×10^{-9} cm W^{-1}	4×10^{-15} esu	>15	4	8×10^{-9} cm^2 W^{-1} M^{-1}	1.1

the valley on the OA z-scans compared with the observed shapes of z-scans. Moreover, these processes can be preferably anticipated in the case of 1064 nm pump. The same can be said about the nonlinear refractivities of higher orders. Note in this connection an interesting feature of the $T(z)$ dependence in the case of CA z-scans related with the third-order nonlinear optical processes. If nonlinear refraction is caused by the third-order nonlinearities, then the distance ΔZ between the transmission maximum and minimum is related to the spatial characteristics of focused radiation in the focal plane by the expression $\Delta Z \cong 1.7z_o$, where z_o is the Rayleigh length of the focused radiation. Thus, the spatial parameters of focused radiation can be obtained with good accuracy from the dependence of the normalized transmission on z upon scanning the sample. In the case of higher-order refractive nonlinearity, the coefficient 1.7 in above formula decreases down to 1.4, which means that ΔZ becomes smaller and CA z-scan looks narrower. In our studies, we did not observe a decrease of ΔZ in the used range of probe pulse intensities.

Another issue here is the application of these QDs for high-order harmonics generation. Actually, this process cannot be described by the perturbative regime of laser-matter interaction. So the determination of the parameters of high-order harmonic generation in the media containing quantum dots cannot be attributed to the definition of the high-order nonlinearities of those species.

As it was metioned, QDs were used as the efficient media for high-order harmonics generation in the extreme ultraviolet range [19,21]. Knowing the low-order nonlinearities of QDs allows determining the optimal conditions of excitation of these species for efficient generation of harmonics. Some QDs, like metal sulfides showed strong low-order nonlinearities, while also demonstrating efficient generation properties as the emitters of harmonics in the 20–100 nm range. Particularly, the nonlinear refraction index and nonlinear absorption coefficient of $Cd_{0.5}Zn_{0.5}S$ alloyed quantum dots were measured at $\lambda = 1064$ nm to be 2×10^{-13} cm^2 W^{-1} and 1.2×10^{-8} cm W^{-1}, while RSA of $Cd_{0.5}Zn_{0.5}S$ quantum dots at $\lambda = 532$ nm was almost two orders larger [22]. The application of these QDs for generation of coherent extreme ultraviolet allowed for demonstration of two-color pump induced growth of harmonic generation efficiency [19]. Similar observation has been reported in the case of Ag_2S QDs, which have shown strong nonlinear refraction and absorption [23,24], as well as the efficient generation of high-order harmonics [21]. These observations allow expecting the attractive properties of the studied HgSe CQDs as the emitters of high-order harmonics.

5. Conclusions

Two methods for the synthesis of mercury selenide colloidal QDs were studied in detail and compared. Dependence of the position of intraband absorption peak in HgSe colloidal quantum

dots on the ratio of Hg and Se precursors as well as reaction temperature was established. HgSe CQDs with mean size from 5 to 11 nm and intraband absorption peak from 3.7 μm up to 10 μm were prepared. In general, quantum dots prepared from of Hg-precursor, obtained by subsequent addition, demonstrated better colloidal stability and narrower intraband absorption peaks. It was found that a prolonged heating or high temperatures (>100 °C) by mercury precursor preparation lead to the formation of large amount of metallic mercury as a side product. The best particles size distribution was observed at the synthesis at 100 °C with 1:1 Hg:Se ratio. These particles were applied for the nonlinear optical studies.

The negative nonlinear refraction (γ = -5×10^{-12} cm^2 W^{-1}) and nonlinear absorption (β = 6×10^{-7} cm W^{-1}) of colloidal quantum dots were determined using 10 ns, 532 nm laser radiation. The joint influence of above processes was realized at higher intensity of probe pulses. In the case of 10 ns, 1064 nm radiation, only negative nonlinear refraction dominated during z-scan studies of these quantum dots. The studies of optical limiting using two laser sources demonstrated the effectiveness of this process at λ=532 nm. The role of nonlinear scattering is analyzed. We discussed the mechanisms responsible for the nonlinear optical processes in colloidal HgSe quantum dots.

Disclosures. The authors declare no conflicts of interest.

Data availability. Data underlying the results presented in this paper are not publicly available at this time but may be obtained from the authors upon reasonable request.

References

1. L. W. Liu, S. Hu, Y. P. Dou, T. H. Liu, J. Q. Lin, and Y. Wang, "Nonlinear optical properties of near-infrared region Ag$_2$S quantum dots pumped by nanosecond laser pulses," Beilstein J. Nanotechnol. **6**(8), 1781–1787 (2015).
2. P. Kumbhakar, M. Chattopadhyay, and A. K. Mitra, "Nonlinear optical properties of doped ZnS quantum dots," Int. J. Nanosci. **10**(01n02), 177–180 (2011).
3. Z. Zeng, C. S. Garoufalis, A. F. Terzis, and S. Baskoutas, "Linear and nonlinear optical properties of ZnS/ZnO core shell quantum dots: effect of shell thickness, impurity, and dielectric environment," J. Appl. Phys. **114**(2), 023510 (2013).
4. H. Linnenbank, Y. Grynko, J. Förstner, and S. Linden, "Second harmonic generation spectroscopy on hybrid plasmonic/dielectric nanoantennas," Light: Sci. Appl. **5**(1), e16013 (2016).
5. R. B. Martin, M. J. Meziani, P. Pathak, J. E. Riggs, D. E. Cook, S. Perera, and Y.-P. Sun, "Optical limiting of silver-containing nanoparticles," Opt. Mater. **29**(7), 788–793 (2007).
6. R. Karimzadeh, H. Aleali, and N. Mansour, "Thermal nonlinear refraction properties of Ag2S semiconductor nanocrystals with its application as a low power optical limiter," Opt. Commun. **284**(9), 2370–2375 (2011).
7. X. Liu, Y. Adachi, Y. Tomita, J. Oshima, T. Nakashima, and T. Kawai, "High-order nonlinear optical response of a polymer nanocomposite film incorporating semiconducotor CdSe quantum dots," Opt. Express **20**(12), 13457–13469 (2012).
8. S. Abe, J. J. Joos, L. I. D. J. Martin, Z. Hens, and P. F. Smet, "Hybrid remote quantum dot/powder phosphor designs for display backlights," Light: Sci. Appl. **6**(6), e16271 (2017).
9. R. A. Ganeev, A. I. Ryasnyansky, A. L. Stepanov, and T. Usmanov, "Nonlinear optical susceptibilities of copper- and silver - doped silicate glasses in the ultraviolet range," Phys. Status Solidi B **238**(2), R5–R7 (2003).
10. R. A. Ganeev, A. I. Ryasnyansky, R. I. Tugushev, and T. Usmanov, "Investigation of nonlinear refraction and nonlinear absorption of semiconductor nanoparticles solutions prepared by laser ablation," J. Opt. A: Pure Appl. Opt. **5**(4), 409–417 (2003).
11. A. Rout, G. S. Boltaev, R. Ganeev, K. S. Rao, D. Fu, R. Rakhimov, S. Kurbanov, S. Urolov, Z. Shaymardanov, and C. Guo, "Low- and high-order nonlinear optical studies of ZnO nanocrystals, nanoparticles and nanorods," Eur. Phys. J. D **73**(11), 235 (2019).
12. R. A. Ganeev, G. S. Boltaev, V. V. Kim, and C. Guo, "Effects of laser plasma formation on quasi-phase matching of high-order harmonics from nanoparticles and atoms," Nanomaterials **9**(4), 572 (2019).
13. R. A. Ganeev, M. Baba, A. I. Ryasnyansky, M. Suzuki, and H. Kuroda, "Laser ablation of GaAs in liquids: structural, optical, and nonlinear optical characteristics of colloidal solutions," Appl. Phys. B **80**(4-5), 595–601 (2005).
14. R. A. Ganeev, A. I. Ryasnyanskiy, and T. Usmanov, "Optical and nonlinear optical characteristics of the Ge and GaAs nanoparticles suspensions prepared by laser ablation," Opt. Commun. **272**(1), 242–246 (2007).
15. G. Fan, S. Qu, Q. Wang, C. Zhao, L. Zhang, and Z. Li, "Pd nanoparticles formation by femtosecond laser irradiation and the nonlinear optical properties at 532 nm using nanosecond laser pulses," J. Appl. Phys. **109**(2), 023102 (2011).

16. R. A. Ganeev, A. I. Ryasnyansky, A. L. Stepanov, and T. Usmanov, "Saturated absorption and reverse saturated absorption of Cu:SuO2 at (=532 nm," Phys. Status Solidi B **241**(3), R1–R4 (2004).

17. R. A. Ganeev, M. Suzuki, M. Baba, M. Ichihara, and H. Kuroda, "Low- and high-order nonlinear optical properties of Au, Pt, Pd, and Ru nanoparticles," J. Appl. Phys. **103**(6), 063102 (2008).

18. J. V. Antony, J. J. Pillai, P. Kurian, V. N. Nampoori, and G. E. Kochimoolayil, "Photoluminescence and optical nonlinearity of CdS quantum dots synthesized in a functional copolymer hydrogel template," New J. Chem. **41**(9), 3524–3536 (2017).

19. R. A. Ganeev, G. S. Boltaev, V. V. Kim, M. Venkatesh, A. I. Zvyagin, M. S. Smirnov, O. V. Ovchinnikov, M. Wöstmann, H. Zacharias, and C. Guo, "High-order harmonic generation using quasi-phase matching and two-color pump of the plasmas containing molecular and alloyed metal sulfide quantum dots," J. Appl. Phys. **126**(19), 193103 (2019).

20. B. Zhu, F. Wang, C. Liao, H. Zhang, J. Zhang, Y. Cui, Y. Ye, and Y. Gu, "Size confinement and origins of two-photon absorption and refraction in CdSe quantum dots," Opt. Express **27**(3), 1777–1785 (2019).

21. R. A. Ganeev, G. S. Boltaev, V. V. Kim, K. Zhang, A. I. Zvyagin, M. S. Smirnov, O. V. Ovchinnikov, P. V. Redkin, M. Wöstmann, H. Zacharias, and C. Guo, "Effective high-order harmonic generation from metal sulfide quantum dots," Opt. Express **26**(26), 35013–35025 (2018).

22. G. S. Boltaev, B. Sobirov, S. Reyimbaev, H. Sherniyozov, T. Usmanov, M. S. Smirnov, O. V. Ovchinnikov, I. G. Grevtseva, T. S. Kondratenko, H. S. Shihaliev, and R. A. Ganeev, "Nonlinear optical characterization of colloidal solutions containing dye and Ag$_2$S quantum dot associates," Appl. Phys. A **122**(12), 999 (2016).

23. T. S. Kondratenko, M. S. Smirnov, O. V. Ovchinnikov, A. I. Zvyagin, R. A. Ganeev, and G. Grevtseva, "Nonlinear optical properties of hybrid associates of Ag$_2$S quantum dots with erythrosine molecules," Optik **200**(16), 163391 (2020).

24. A. I. Zvyagin, T. Chevychelova, I. Grevtseva, M. S. Smirnov, A. S. Selyukov, O. V. Ovchinnikov, and R. A. Ganeev, "Nonlinear refraction in colloidal silver sulfide quantum dots," J. Russ. Laser Res. **41**(6), 670–680 (2020).

25. M. Chen, G. Shen, and P. Guyot-Sionnest, "Size distribution effects on mobility and intraband gap of HgSe quantum dots," J. Phys. Chem. C **124**(29), 16216–16221 (2020).

26. W. B. Gao, P. Fallahi, E. Togan, J. Miguel-Sanchez, and A. Imamoglu, "Observation of entanglement between a quantum dot spin **and a** single photon," Nature **491**(7424), 426–430 (2012).

27. H. Mirzai and M. Green, "Synthetic routes to mercury chalcogenide quantum dots," J. Mater. Chem. C **6**(19), 5097–5112 (2018).

28. D. D. Torres, S. Pamidighantam, and P. K. Jain, "Crystal symmetry, strain, and facet-dependent nature of topological surface states in mercury selenide," J. Phys. Chem. C **124**(19), 10344–10352 (2020).

29. Z. Deng, K. K. S. K. Jeong, and P. Guyot-Sionnest, "Colloidal quantum dots intraband photodetectors," ACS Nano **8**(11), 11707–11714 (2014).

30. X. Tang, G. F. Wu, and K. W. C. Lai, "Plasmon resonance enhanced colloidal HgSe quantum dots filterless narrowband photodetectors for mid-wave Infrared," J. Mater. Chem. C **5**(2), 362–369 (2017).

31. S. B. Hafiz, M. Scimeca, A. Sahu, and D.-K. Ko, "Colloidal quantum dots for thermal infrared sensing and imaging," Nano Convergence **6**(1), 7 (2019).

32. J. Jeong, B. Yoon, Y.-W. Kwon, D. Choi, and K. S. Jeong, "Singly and doubly occupied higher quantum state in nanocrystals," Nano Lett. **17**(2), 1187–1193 (2017).

33. R. A. Ganeev, A. I. Ryasnyansky, A. L. Stepanov, and T. Usmanov, "Characterization of nonlinear-optical parameters of copper- and silver-doped silica glasses at (=1064 nm," Phys. Status Solidi B **241**(4), 935–944 (2004).

34. R. A. Ganeev, M. Baba, M. Morita, D. Rau, H. Fujii, A. I. Ryasnyansky, N. Ishizawa, M. Suzuki, and H. Kuroda, "Nonlinear optical characteristics of CdS and ZnS nanoparticles doped in zirconium oxide films," J. Opt. A: Pure Appl. Opt. **6**(4), 447–453 (2004).

35. T. Karali, N. Can, L. Valberg, A. L. Stepanov, P. D. Townsend, C. Buchal, R. A. Ganeev, A. I. Ryasnyansky, H. G. Belik, M. L. Jessett, and C. Ong, "Optical properties and luminescence of metallic nanoclusters in ZnO:Cu," Phys. B **363**(1-4), 88–95 (2005).

36. C. Melnychuk and P. Guyot-Sionnest, "Auger suppression in n-type HgSe colloidal quantum dots," ACS Nano **13**(9), 10512–10519 (2019).

37. N. Goubet, C. Livache, B. Martinez, X. Z. Xu, S. Ithurria, S. Royer, H. Cruguel, G. Patriarche, A. Ouerghi, M. Silly, B. Dubertret, and E. Lhuillier, "Wave-function engineering in HgSe/HgTe colloidal heterostructures to enhance mid-infrared photoconductive properties," Nano Lett. **18**(7), 4590–4597 (2018).

38. B. Martinez, C. Livache, L. D. Notemgnou Mouafo, N. Goubet, S. Keuleyan, H. Cruguel, S. Ithurria, H. Aubin, A. Ouerghi, B. Doudin, E. Lacaze, B. Dubertret, M. G. Silly, R. P. S. M. Lobo, J.-F. Dayen, and E. Lhuillier, "HgSe self-doped nanocrystals as a platform to investigate the effects of vanishing confinement," ACS Appl. Mater. Interfaces **9**(41), 36173–36180 (2017).

39. C. Livache, B. Martinez, N. Goubet, C. Gréboval, J. Qu, A. Chu, A. S. Royer, S. Ithurria, M. G. Silly, B. Dubertret, and E. Lhuillier, "A colloidal quantum dot infrared photodetector and its use for intraband detection," Nat. Commun. **10**(1), 2125 (2019).

40. M. Chen, G. Shen, and P. Guyot-Sionnest, "State-resolved mobility of 1 cm^2/(Vs) with HgSe quantum dot films," J. Phys. Chem. Lett. **11**(6), 2303–2307 (2020).

41. A. Robin, C. Livache, S. Ithurria, E. Lacaze, B. Dubertret, and E. Lhuillier, "Surface control of doping in self-doped nanocrystals," ACS Appl. Mater. Interfaces **8**(40), 27122–27128 (2016).

42. E. Lhuillier, M. Scarafagio, P. Hease, B. Nadal, H. Aubin, X. Zhen Xu, N. Lequeux, G. Patriarche, S. Ithurria, and B. Dubertret, "Infrared photodetection based on colloidal quantum-dot films with high mobility and optical absorption up to THz," Nano Lett. **16**(2), 1282–1286 (2016).

43. I. A. Shuklov, I. S. Mikhel, A. V. Nevidimov, K. P. Birin, N. V. Dubrovina, A. A. Lizunova, and V. F. Razumov, "Mechanistic insights into the synthesis of telluride colloidal quantum dots with trioctylphosphine-tellurium," ChemistrySelect **5**(28), 11896–11900 (2020).

44. I. A. Shuklov, V. F. Toknova A, A. Lizunova, and V. F. Razumov, "Controlled aging of PbS colloidal quantum dots under mild conditions," Mater. Today Chem. **18**(10), 100357 (2020).

45. S. B. Brichkin and V. F. Razumov, "Colloidal quantum dots: synthesis, properties and applications," Russ. Chem. Rev. **85**(12), 1297–1312 (2016).

46. I. A. Shuklov and V. F. Razumov, "Lead chalcogenide quantum dots for photoelectric devices," Russ. Chem. Rev. **89**(3), 379–391 (2020).

47. L. Liu, Q. Wu, Y. Ding, H. Liu, and B. Zhang, "Synthesis of HgSe quantum dots through templates controlling and gas–liquid transport with emulsion liquid membrane system," Colloids Surf., A **240**(1-3), 135–139 (2004).

48. R. W. Boyd, "The intensity-dependent refractive index," In *Nonlinear Optics; 189–235*, Elsevier, Amsterdam, The Netherlands (2003).

49. M. Sheik-Bahae, A. A. Said, T. H. Wei, D. J. Hagan, and E. W. Van Stryland, "Sensitive measurement of optical nonlinearities using a single beam," IEEE J. Quantum Electron. **26**(4), 760–769 (1990).

50. X. Liu, S. Guo, H. Wang, and L. Hou, "Theoretical study on the closed-aperture Z-scan curves in the materials with nonlinear refraction and strong nonlinear absorption," Opt. Commun. **197**(4-6), 431–437 (2001).

51. M. Sheik-Bahae, A. A. Said, and E. W. Van Stryland, "High-sensitivity, single-beam n2 measurements," Opt. Lett. **14**(17), 955–957 (1989).

52. R. Jin, Y. Cao, C. A. Mirkin, K. L. Kelly, G. C. Schatz, and J. G. Zheng, "Photoinduced conversion of silver nanospheres to nanoprisms," Science **294**(5548), 1901–1903 (2001).

53. A. I. Zvyagin, A. S. Perepelitsa, M. S. Lavlinskaya, O. V. Ovchinnikov, M. S. Smirnov, and R. A. Ganeev, "Demonstration of variation of the nonlinear optical absorption of non-spherical silver nanoparticles," Optik **175**(1), 93–98 (2018).

54. J. He, L. Tao, H. Zhang, B. Zhou, and J. Li, "Emerging 2D materials beyond graphene for ultrashort pulse generation in fiber lasers," Nanoscale **11**(6), 2577–2593 (2019).

55. H. Yuan, F. Zhu, J. Wang, R. Yang, N. Wang, Y. Yu, P. Yan, and J. Guo, "Generation of ultra-fast pulse based on bismuth saturable absorber," Wuli Xuebao **69**(9), 094203 (2020).

56. G. Liu, F. Zhang, T. Wu, Z. Li, W. Zhang, K. Han, F. Xing, Z. Man, X. Ge, and S. Fu, "Single- and dual-wavelength passively mode-locked erbium-doped fiber laser based on antimonene saturable absorber," IEEE Photonics J. **11**(3), 1–11 (2019).

57. L. Lu, X. Tang, R. Cao, L. Wu, Z. Li, G. Jing, B. Dong, S. Lu, Y. Li, Y. Xiang, J. Li, D. Fan, and H. Zhang, "Broadband nonlinear optical response in few-layer antimonene and antimonene quantum dots: a promising optical Kerr media with enhanced stability," Adv. Opt. Mater. **5**(17), 1700301 (2017).

58. F. Zhang, G. Liu, Z. Wang, T. Tang, X. Wang, C. Wang, S. Fu, F. Xing, K. Han, and X. Xu, "Broadband nonlinear absorption properties of two-dimensional hexagonal tellurene nanosheets," Nanoscale **11**(36), 17058–17064 (2019).

59. L. Wu, Y. Dong, J. Zhao, D. Ma, W. Huang, Y. Zhang, Y. Wang, X. Jiang, Y. Xiang, J. Li, Y. Feng, J. Xu, and H. Zhang, "Kerr nonlinearity in 2D graphdiyne for passive photonic diodes," Adv. Mater. **31**(14), 1807981 (2019).

60. B. Wang, S. Zhong, Y. Ge, H. Wang, X. Luo, and H. Zhang, "Present advances and perspectives of broadband photo-detectors based on emerging 2D-Xenes beyond graphene," Nano Res. **13**(4), 891–918 (2020).

61. I. D. Skurlov, E. A. Ponomareva, A. O. Ismagilov, S. E. Putilin, I. A. Vovk, A. V. Sokolova, A. N. Tcypkin, and A. P. Litvin, "Size dependence of the resonant third-order nonlinear refraction of colloidal PbS quantum dots," Photonics **7**(2), 39 (2020).

62. M. Sheik-Bahae, D. C. Hutchings, D. J. Hagan, and E. W. Van Stryland, "Dispersion of bound electronic nonlinear refraction in solids," IEEE J. Quantum Electron. **27**(6), 1296–1309 (1991).

63. M. Cardona, R. K. Kremer, R. Lauck, G. Siegle, A. Muñoz, and A. H. Romero, "Electronic, vibrational, and thermodynamic properties of metacinnabar β-HgS, HgSe, and HgTe," Phys. Rev. B **80**(19), 195204 (2009).

64. L. Brzozovski and E. H. Sargent, "Azobenzenes for photonic network Applications: third-order nonlinear optical properties," J. Mater. Sci.: Mater. Electron. **12**(9), 483–489 (2001).